HHS Public Access

Author manuscript

J Colloid Interface Sci. Author manuscript; available in PMC 2021 September 30.

Published in final edited form as:

J Colloid Interface Sci. 2021 March ; 585: 668–675. doi:10.1016/j.jcis.2020.10.046.

Flexible-templated imprinting for fluorine-free, omniphobic plastics with re-entrant structures

Xiaoxiao Zhao[a], **Daniel S. Park**[a], **Junseo Choi**[a], **Sungook Park**[a], **Steven A. Soper**[b], **Michael C. Murphy**[a,*]

[a]Center for BioModular Multiscale Systems for Precision Medicine, Department of Mechanical & Industrial Engineering, Louisiana State University, Baton Rouge, LA 70803, United States

[b]Departments of Chemistry and Mechanical Engineering, University of Kansas, Lawrence, KS 66045, United States

Abstract

Hypothesis: Compared to vertical micro-pillars, re-entrant micro-structures exhibited superior omniphobicity for suspending liquids to Cassie-Baxter state. However, the existing re-entrant structures rely on complex multi-step deposition and etching procedures. The conventional, rigid-templated imprinting would instead damage the re-entrant structures. This leads to the question: is it possible to preserve the re-entrant curvatures by a flexible-templated imprinting?

Experiments: We facilely imprinted the re-entrant structures on a plastic substrate using a flexible nylon-mesh template. The effect of imprinting time (15–35 min), temperature (110–120 °C) and pressure (15–50 Bar) was investigated. To further improve the liquid-repellency and abrasion resistance, the silica nanoparticles (30–650 nm) along with epoxy resin binder (10 mg/mL) were pre-coated.

Findings: A one-step imprinting is sufficient to fabricate the re-entrant structures by utilizing flexible nylon-mesh template, without damaging the imprinted structures after the demolding process. The pre-coated silica nanoparticles and epoxy resin (1) improved liquid repellency by introducing hierarchical surface structures (e.g. contact angle hysteresis of olive oil reduced > 10°), and (2) acted as a protective layer against mechanical abrasion (omniphobicity maintained after 25 cycles, ~1.6 kPa sand paper abrasion). Additionally, the fluorine-free post-treatment was sufficient for the omniphobicity on the obtained plastic structures.

GRAPHICAL ABSTRACT

*Corresponding author. murphy@lsu.edu (M.C. Murphy).

CRediT authorship contribution statement

Xiaoxiao Zhao: Conceptualization, Methodology, Writing - original draft. **Daniel S. Park:** Writing - review & editing. **Junseo Choi:** Writing - review & editing. **Sungook Park:** Writing - review & editing. **Steven A. Soper:** Writing - review & editing. **Michael C. Murphy:** Conceptualization, Writing - review & editing.

Declaration of Competing Interest

The authors declare that they have no known competing financial interests or personal relationships that could have appeared to influence the work reported in this paper.

Declaration of Competing Interest

The authors declare no conflict of interest.

Appendix A. Supplementary material

Supplementary data to this article can be found online at https://doi.org/10.1016/j.jcis.2020.10.046.

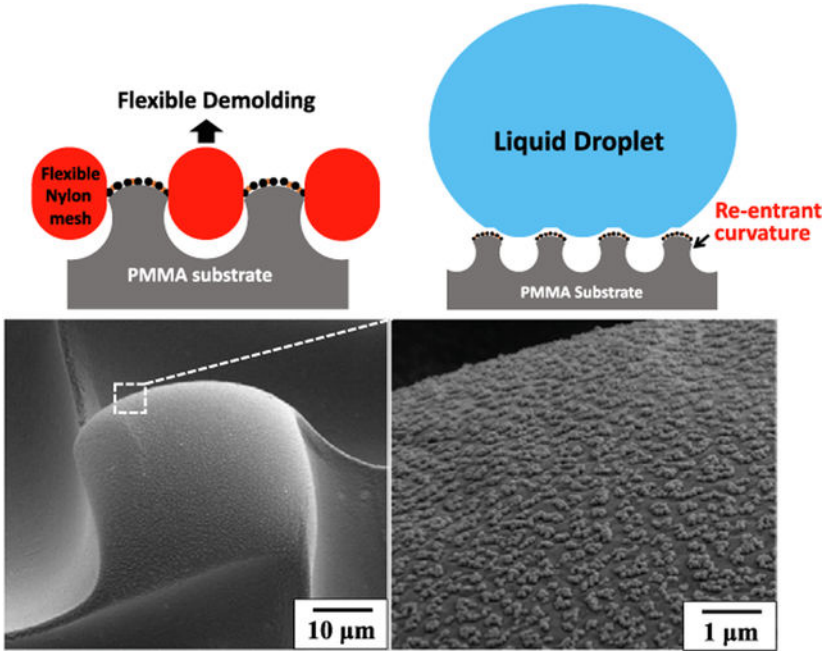

Keywords

Omniphobic; Re-entrant structure; Plastics; Nanoparticles; Template imprinting

1. Introduction

A surface that repels essentially all liquids, such as water and various oils, has a wide range of applications, including self-cleaning, corrosion prevention, stain-free apparel, and paper packaging [1–4]. Omniphobic surfaces exhibit a high contact angle (CA) and a low contact angle hysteresis (CAH) with both high and low surface tension liquids [5]. However, it is challenging to maintain a stable Cassie-Baxter state on such surfaces, especially for trapping microscopic air beneath the low surface tension liquids. Previous studies have shown that re-entrant (or convex) structures inhibit the penetration of low-surface-tension liquids into the surface air cavities, which prevents a fully wetted Wenzel state. This is achieved by tailoring the convex angle of the re-entrant geometries to be lower than Young's contact angle of the probe liquids, which generates an upward net force on the composite (liquid–air) interface due to the capillary action [5,6]. However, it requires multi-step deposition and selective etching procedures to obtain such re-entrant or doubly re-entrant geometries [7,8], which limits their large-scale applications. It is favorable to develop a low cost and facile strategy to fabricate re-entrant geometries for omniphobic surfaces.

In addition to re-entrant geometries, hierarchical surface structures further reduce solid–liquid contact area in Cassie-Baxter state, resulting in a lower CAH for omniphobic surfaces [9]. Without hierarchical structures, previous studies have shown that the bare re-entrant micro-pillars exhibited a relatively high CAH for a wide range of liquids [10,11]. For obtaining hierarchical structures, it is necessary to roughen a finer length scale texture on the re-entrant geometries. Subtractive nano-texturing methods such as thermal or UV

imprinting, polymer casting, and selective etching may result in fragile surface structures that can be easily damaged by mechanical wear [12–15]. On the other hand, additive nano-texturing methods such as dip coating or spraying high Mohs hardness nanoparticles may temporarily improve the surface wear resistance [16,17]. However, the nanoparticles could be easily detached over time due to their low adhesion strength to substrates. For practical engineering applications, it is necessary to improve the mechanical durability of such nano-textures for developing omniphobic surfaces.

Previous research on the preparation of omniphobic plastics typically utilizes long chain perfluorinated compound (PFCs) for low surface energy treatment [18–20]. However, PFCs may cause persistent environmental and human health concerns, which is especially true considering their exceptional chemical stability [21]. For example, in the United States, the Food and Drug Administration (FDA) have banned three PFC-containing coating materials in food packaging since 2016. Although fluorine-free omniphobic coatings have been reported in the past decade, the fragile and nano-porous surface structures limit their practical applications [22–24]. A non-porous, single layer of nanoparticles along with selective chemical binders may improve the surface wear resistance. However, it may lead to insufficient surface omniphobicity in Wenzel state. There is an immediate demand for fluorine-free, omniphobic plastics, because they are non-toxic, biocompatible, and more favorable in applications such as biomedical microfluidic devices, drink and food containers [25].

In this study, we report a facile nylon-mesh-imprinting lithography to fabricate the re-entrant micro-pillars on polymethylmethacrylate (PMMA) substrates. Owing to the flexibility of the nylon-mesh templates, the re-entrant micro-pillars maintained their convex angles without being damaged during the demolding process. The nylon-mesh imprinting time, temperature and pressure was optimized for the re-entrant micropillars. Silica nanoparticles were firmly adhered on the micro-pillars via epoxy resin binders, creating robust nano-on-micron geometries that are essential for omniphobic surfaces. Additionally, the high Mohs hardness silica coatings are resistant to mechanical abrasion, benefiting their potential engineering applications. The obtained omniphobic surfaces exhibited high liquid-repellency for various liquids such as water, ethylene glycol, and olive oil.

2. Experimental section

2.1. Materials

Nylon mesh (33 μm wire diameter, 17–49% open area) and P1000 sandpaper were purchased from McMaster-Carr. Poly (methyl methacrylate) (PMMA) (Cope Plastics, 100 × 100 mm surface area, 0.75 mm thick) was used as spin-coating substrates. Diglycidyl ether of bisphenol A (DGEBA) was purchased from Electron Microscopy Sciences. 4,4′-diaminodiphenylmethane (DDM) was brought from TCI America. Anhydrous ethanol was obtained from Decon Laboratories (200 proof). Trichloro-octadecylsilane (OTS) was received from VWR International (Radnor, PA). Perfluorodecyltrichlorosilane (FDTS) was obtained from Gelest, Inc.

2.2. Fabrications of nano-on-micron structures

First, nanostructures were obtained by spin coating a mixture of silica particles and epoxy resin. Briefly, silica particles of 32 ± 3 nm, 73 ± 6 nm, 207 ± 8 nm, 411 ± 13 nm, and 653 ± 15 nm were synthesized via Stöber method, as detailed in our previous studies [26]. The epoxy resin was prepared by mixing epoxy (DGEBA) and amine curing agent (DDM) with a 2:1 M ratio. The 500 mg silica particles (30 to 650 nm) were dispersed in an 20 mL ethanol solution of epoxy resin (10 mg/mL) to obtain spin coating mixture. After sonication for 30 min, the mixture was spin coated (Bidtex SP100 spin coater) onto PMMA substrate at 2000 rpm for 60 s. The coating film was then cured in 90 °C oven for 1 h.

Second, microstructures were obtained by imprinting nylon-mesh template onto the nanostructured PMMA substrate using a commercial nanoimprint lithography (NIL) machine (Obducat 6-inch NIL). Briefly, NIL imprinting was performed at 115 °C, 35 Bar for 15 min, expect when altering imprinting parameters intentionally for Fig. 2a–c. The system was then cooled down to 70 °C during demolding process. The PMMA substrate was then oxygen plasma (30 W, 0.15 Torr, Harrick Plasma PDC-32G) treated for 1 min, followed by vapor deposition of OTS/FDTS for low energy surface treatment.

2.3. Characterization

The morphology of the structured PMMA surfaces was analysed using a Field Emission Gun Scanning Electron Microscope (FEG-SEM, The quanta 3D DualBeam). Prior to SEM imaging, the conductivity of the samples was improved by sputtering a layer of 10 nm platinum (EMS550X sputter coater) to reduce charging effect. The apparent CA and CAH were measured by a VCR Optima goniometer (AST Products, Inc.) using a droplet shape software (VCA Optima XE). Apparent CA was measured with droplets of 10 μL distilled water deposited onto samples with a microsyringe. CAH was recorded as the difference of the advancing and receding CAs, which is achieved by adding and removing liquid from the sample surface, and the volume of the liquid droplet was 10 μL. Five different positions on each sample were measured [27–29].

3. Results and discussion

3.1. Overall procedures

Mechanically robust, omniphobic surfaces were fabricated using a facile nylon-mesh-imprinting lithography to create the re-entrant micro-pillars on a polymethylmethacrylate (PMMA) substrate. Briefly, A PMMA substrate was first spin coated with silica nanoparticles, along with epoxy resin as a binder [26]. PMMA was chosen as the substrate because its engineering applications often require non-wetting properties, including solar cell panels, aircraft windows, and fluidic medical devices [30,31]. Silica nanoparticles of 30 to 650 nm were investigated for this work. The PMMA substrate was subsequently imprinted by a nylon-mesh template for creating hierarchical nano-on-micron (silica nanoparticles on re-entrant micro-pillars) structures. The overall spin coating and nylon-mesh-imprinting procedures were illustrated in Fig. 1a–c (see Experimental Section for details). After vapor deposition of trichloro-octadecylsilane (OTS)

or perfluorodecyltrichlorosilane (FDTS), the obtained surface is capable of resisting various liquids in Cassie-Baxter state (Fig. 1d).

3.2. Selection of nylon-mesh sizes

The selection of the nylon-mesh template was based on two design parameters: feature spacing ratio D^* and robustness factor A^* [5]. First, $D^* = [(R + D)/R]^2$ is a measure of the solid–liquid contact fraction, where $2R$ is the diameter of micro-pillars, and $2D$ is the spacing between micro-pillars. Second, $A^* = P_b/P_{ref}$ is a measure of the stability of the Cassie-Baxter state, where P_b is the breakthrough pressure that fully wet the surface, and P_{ref} is the reference pressure. Too low of D^* (<1) would decrease the apparent contact angle, resulting in a reduced liquid repellency. Too high of D^* ($\gg$ 1) would otherwise decrease the robustness factor A^*, leading to an unstable Cassie-Baxter state. Therefore, to obtain a stable Cassie-Baxter state while not significantly compromising the liquid repellency, the imprinting nylon-mesh was selected with $D^* = 4$ (R = 33 μm and D = 33 μm, Fig. 1e–f).

3.3. Template imprinting parameters

We first investigated the effect of imprinting time, pressure, and temperature on the height of the re-entrant micro-pillars. Three imprinting temperatures (110 °C, 115 °C, and 120 °C) was selected to be slightly above the glass transition temperature of PMMA substrates (105 °C). At each imprinting temperature, the height of the re-entrant micro-pillars showed an increasing trend with imprinting time and pressure, as expected (Fig. 2a–c). As a result, low values of the imprinting parameters (time, pressure, and temperature) may cause the incomplete molding and reduced liquid repellency (Fig. 2d and g). However, high values of the imprinting parameters may cause the flattening of top micro-pillars and the embedding the pre-coated nanoparticles (Fig. 2e and h, Figure S1). Further, although the nylon-mesh template was flexible, a complete immersion of nylon-mesh in PMMA substrate at ultra-high imprinting parameters may still lead to the fracture of micro-pillars during demolding (Fig. 2f and i). To avoid the above-mentioned issues, the optimized imprinting parameters (115 °C, 35 Bar for 15 min) were used in this study.

3.4. Liquid repellency of re-entrant and vertical micro-structures

The liquid repellency of our bare re-entrant micro-pillars and the vertical micro-cylinder structure were compared. The micro-cylinders were imprinted as described in the previous studies [32]. According to Young's equation [33], a liquid droplet exhibits an equilibrium contact angle θ_Y when sit on a smooth, solid surface. For a high surface-tension liquid (θ_Y > 90°, Fig. 3a and b), simple vertical micro-cylinders are sufficient to suspend it. However, because the intrinsic oleophobic materials do not exist, re-entrant topologies are required to resist a low surface-tension liquid ($\theta'_Y < 90°$, Fig. 3d and 3e). That is, for the same surface chemistry, adding re-entrant structures allows trapping air underneath the liquids at lower Young's contact angle. The micro-cylinders and re-entrant micro-pillars with the same feature spacing ratio ($D^* = 4$) were fabricated, as shown in SEM images (Fig. 3c and 3f). We measured the apparent CAs and hysteresis of water, ethylene glycol, olive oil, and hexadecane on the fabricated surfaces after post-treatment with both fluorine-free (OTS, Fig. 3g) and fluorinated chemistries (FDTS, Fig. 3h). As expected, the bare re-entrant

micro-pillar surfaces exhibited higher apparent CAs and lower hysteresis, indicating the indispensable role of re-entrant geometries in suspending liquids.

3.5. Nano-on-micron hierarchical structures

Next, we investigated the re-entrant micro-pillars pre-coated with silica nanoparticles with size range from 30 to 650 nm. The spin coating results were not desirable for 30 nm and 650 nm nanoparticles. The 30 nm nanoparticles exhibited smoother surface texture, containing densely packed silica films separated into several pieces (Figure S2). The 650 nm nanoparticles cannot be well dispersed with epoxy resin even under vigorous sonication, resulting in the aggregation of nanoparticles (Figure S3). For this reason, we focused on studying the silica nanoparticles of 70 nm (Fig. 4a–c), 200 nm (Fig. 4d–f), and 400 nm (Fig. 4g–i), respectively. Epoxy resin was used as a binder to adhere the nanoparticles onto the micro-pillars (Inset in Fig. 4i). The epoxy resin concentration (10 mg/mL) was controlled to be high enough for sufficient adhesion while not too high to engulf the nanoparticles. The silica nanoparticles (Mohs hardness of silica is 7 [34]) also worked as a protective coating layer. The spin coating method was chosen as it created a uniform coverage of nanoparticles, while a simple dip coating would lead to the agglomeration of epoxy resin and nanoparticles (Figure S4).

3.6. Effect of the pre-coated silica/epoxy on wettability and durability

We also measured the apparent CA and the hysteresis of water, ethylene glycol, and olive oil on the three fluorine-free, OTS treated surfaces (Fig. 5a–c). The re-entrant micro-pillar surfaces exhibited higher liquid repellency when coated with 70 nm silica nanoparticles. We speculated that the 70 nm nanoparticles allowed smaller solid–liquid contact area in the Cassie-Baxter state, resulting in a higher D^* (Fig. 5d). In comparison, other size range of nanoparticles may reside in mixed-mode Cassie/Wenzel state (such as 200 and 400 nm, Fig. 5e) or completely wetted Wenzel state (such as 30 and 650 nm, Fig. 5f). In addition, to demonstrate the resistance of the silica nanoparticle coatings against mechanical abrasion, the sandpaper test was conducted on both nanoparticle pre-coated and bare micro-pillars. For each abrasion cycle, the PMMA sample surface was moved 20 cm back and forth at a pressure of ~ 1.6 kPa (100 g weight on a 2.5*2.5 cm sample area) on a standard P1000 sandpaper (Fig. 5g). In contrast to the bare micro-pillars, the nanoparticle/epoxy armored PMMA surfaces maintained their repellency to olive oil after 25 cycles (Fig. 5h). Therefore, the high Mohs hardness of the nanoparticles, along with the epoxy resin binder, increased the mechanical robustness of the micro-pillar structured plastics.

4. Conclusions

Several literature papers reported hierarchical nano-on-micron structures, such as using photolithography, thermal and ultraviolet (UV) imprinting, polydimethylsiloxane (PDMS) casting on polymer substrates, or DRIE with silicon-based substrates to create microscale structures, followed by thermal- and UV-imprinting, plasma selective etching with O_2, CF_4, and XeF_2, nanoimprinting or chemical and electrodeposition to obtain nanostructures [12–15,35–40]. For example, Bormashenko et al. [13] hot embossed polyethylene from a steel wire template to create microscale hairy structures, followed by cold CF_4 plasma to create

nanostructures. Nguyen et al. [14] used photolithography and deep reactive iron etching (DRIE) to create micropillar structures, followed by metal-assisted electroless etching or chemical vapor deposition (CVD) of silicon nanowire to create nanostructures. Kwon et al. [36] conducted deep reactive ion etching to fabricate micropillars on silicon surfaces, followed by isotropic XeF_2 etching to create a uniform nanotextures. Sung et al. [38] conducted nanoimprinting on a thermal shrinkage film to fabricate nanopillar structures, followed by annealing process to shrink the film to obtain wrinkled microstructures. Wagterveld et al. [39] used excimer laser ablation to pattern micropillars on photoresist SU-8 and nanosized debris were simultaneously generated to obtain nanostructures. However, none of the above nano-on-micron structures exhibited re-entrant structures and therefore exhibited compromised oil repellency. In addition, the nanostructures obtained by etching or imprinting have limited mechanical durability. By far, no studies have yet facilely fabricated the durable, fluorine-free, hierarchical nano-on-micron structures with re-entrant structures.

In summary, we have successfully fabricated the re-entrant structures on PMMA substrates via a one-step nylon-mesh-imprinting lithography. By optimizing the imprinting time, temperature, and pressure, the convex angle of the micro-pillars was maintained after the demolding of the flexible nylon-mesh template. Also, the nylon-mesh template is commercially available and inexpensive, in contrast to previous fabrication methods using multi-step deposition and etching procedures. The pre-coated silica nanoparticles and epoxy resin binder introduced the nano-textures on the re-entrant structures, as well as functioning as an armor against mechanical abrasion. Additionally, it has been shown that a fluorine-free post-treatment was sufficient for the surface omniphobicity. Since it is feasible to fabricate re-entrant structures via the one-step imprinting, we envision that a higher re-entrant curvature may be achievable by tailoring the shape and flexibility of the templates in the future.

Supplementary Material

Refer to Web version on PubMed Central for supplementary material.

Acknowledgments

This project was supported by the LSU Department of Mechanical & Industrial Engineering, the Roy O. Martin Jr. Lumber Co. Professorship of Mechanical Engineering, the National Institute of Biomedical Imaging and Bioengineering of the National Institutes of Health through a research grant R01-EB-010087 and a Biotechnology Resource Center Grant P41-EB-020594, and the State of Louisiana Board of Regents Enhancement Program (LEQSF(2006-07)-ENH-TR-20) and the Louisiana Governor’s Biotechnology Initiative.

Abbreviations:

SEM	Scanning Electron Microscopy
CA	contact angle
CAH	contact angle hysteresis
DGEBA	Diglycidyl ether of bisphenol A

DDM	4,4′-diaminodiphenylmethane
PMMA	poly(methyl methacrylate)
OTS	trichloro-octadecylsilane
NIL	nanoimprint lithography
FDTS	perfluorodecyltrichlorosilane

References

[1]. Pan S, Kota AK, Mabry JM, Tuteja A, Superomniphobic Surfaces for Effective Chemical Shielding, J. Am. Chem. Soc135 (2013) 578–581, 10.1021/ja310517s. [PubMed: 23265660]

[2]. Kota AK, Li Y, Mabry JM, Tuteja A, Hierarchically Structured Superoleophobic Surfaces with Ultralow Contact Angle Hysteresis, Adv. Mater24 (2012) 5838–5843, 10.1002/adma.201202554. [PubMed: 22930526]

[3]. Kota AK, Kwon G, Tuteja A, The design and applications of superomniphobic surfaces e109 e109, NPG Asia Mater6 (2014), 10.1038/am.2014.34.

[4]. Zhao X, Khandoker MAR, Golovin K, Non-Fluorinated Omniphobic Paper with Ultralow Contact Angle Hysteresis, ACS Appl. Mater. Interfaces12 (2020) 15748–15756, 10.1021/acsami.0c01678. [PubMed: 32142254]

[5]. Tuteja A, Choi W, Mabry JM, McKinley GH, Cohen RE, Robust omniphobic surfaces, Proc. Natl. Acad. Sci105 (2008) 18200–18205, 10.1073/pnas.0804872105. [PubMed: 19001270]

[6]. Nosonovsky M, Multiscale roughness and stability of superhydrophobic biomimetic interfaces, Langmuir23 (2007), 10.1021/la062301d.

[7]. Tuteja A, Choi W, Ma ML, Mabry JM, Mazzella SA, Rutledge GC, McKinley GH, Cohen RE, Designing Superoleophobic Surfaces, Science (80-.)318 (2007) 1618–1622. 10.1126/science.1148326.

[8]. Liu T, Kim C-J, Turning a surface superrepellent even to completely wetting liquids, Science80 (2014) 346.

[9]. Golovin K, Lee DH, Mabry JM, Tuteja A, Transparent, Flexible, Superomniphobic Surfaces with Ultra-Low Contact Angle Hysteresis, Angew. Chemie Int. Ed52 (2013) 13007–13011, 10.1002/anie.201307222.

[10]. Choi J, Jo W, Lee SY, Jung YS, Kim SH, Kim HT, Flexible and Robust Superomniphobic Surfaces Created by Localized Photofluidization of Azopolymer Pillars, ACS Nano11 (2017), 10.1021/acsnano.7b01783.

[11]. Wang W, Salazar J, Vahabi H, Joshi-Imre A, Voit WE, Kota AK, Metamorphic Superomniphobic Surfaces, Adv. Mater29 (2017) 1700295, 10.1002/adma.201700295.

[12]. Marquez-Velasco J, Vlachopoulou ME, Tserepi A, Gogolides E, Stable superhydrophobic surfaces induced by dual-scale topography on SU-8, Microelectron. Eng87 (2010) 782–785, 10.1016/j.mee.2009.11.113.

[13]. Bormashenko E, Grynyov R, Chaniel G, Taitelbaum H, Bormashenko Y, Robust technique allowing manufacturing superoleophobic surfaces, Appl. Surf. Sci270 (2013) 98–103, 10.1016/j.apsusc.2012.12.124.

[14]. Nguyen TPN, Boukherroub R, Thomy V, Coffinier Y, Micro-and nanostructured silicon-based superomniphobic surfaces, J. Colloid Interface Sci416 (2014) 280–288, 10.1016/j.jcis.2013.10.065. [PubMed: 24370432]

[15]. Darmanin T, Guittard F, Amigoni S, Tafin De Givenchy E, Noblin X, Kofman R, Celestini F, Superoleophobic behavior of fluorinated conductive polymer films combining electropolymerization and lithography, Soft Matter7 (2011) 1053–1057, 10.1039/C0SM00837K.

[16]. Ebert D, Bhushan B, Wear-resistant rose petal-effect surfaces with superhydrophobicity and high droplet adhesion using hydrophobic and hydrophilic nanoparticles, J. Colloid Interface Sci384 (2012), 10.1016/j.jcis.2012.06.070.

[17]. Xiao Z, Guo H, He H, Liu Y, Li X, Zhang Y, Yin H, Volkov AV, He T, Unprecedented scaling/fouling resistance of omniphobic polyvinylidene fluoride membrane with silica nanoparticle coated micropillars in direct contact membrane distillation, J. Memb. Sci599 (2020), 10.1016/j.memsci.2020.117819.

[18]. Wang J, Kato K, Blois AP, Wong TS, Bioinspired Omniphobic Coatings with a Thermal Self-Repair Function on Industrial Materials, ACS Appl. Mater. Interfaces (2016), 10.1021/acsami.6b00194.

[19]. Leslie DC, Waterhouse A, Berthet JB, Valentin TM, Watters AL, Jain A, Kim P, Hatton BD, Nedder A, Donovan K, Super EH, Howell C, Johnson CP, Vu TL, Bolgen DE, Rifai S, Hansen AR, Aizenberg M, Super M, Aizenberg J, Ingber DE, A bioinspired omniphobic surface coating on medical devices prevents thrombosis and biofouling, Nat. Biotechnol (2014), 10.1038/nbt.3020.

[20]. Pendurthi A, Movafaghi S, Wang W, Shadman S, Yalin AP, Kota AK, Fabrication of Nanostructured Omniphobic and Superomniphobic Surfaces with Inexpensive CO 2 Laser Engraver, ACS Appl. Mater. Interfaces9 (2017) 25656–25661, 10.1021/acsami.7b06924. [PubMed: 28731320]

[21]. Picó Y, Farré M, Llorca M, Barceló D, Perfluorinated Compounds in Food: A Global Perspective, Crit. Rev. Food Sci. Nutr51 (2011) 605–625, 10.1080/10408391003721727. [PubMed: 21793724]

[22]. Cai R, De Smet D, Vanneste M, Nysten B, Glinel K, Jonas AM, One-Step Aqueous Spraying Process for the Fabrication of Omniphobic Fabrics Free of Long Perfluoroalkyl Chains, ACS Omega4 (2019) 16660–16666, 10.1021/acsomega.9b02583. [PubMed: 31616848]

[23]. Khan A, Huang K, Sarwar MG, Rabnawaz M, High modulus, fluorine-free self-healing anti-smudge coatings, Prog. Org. Coatings145 (2020), 10.1016/j.porgcoat.2020.105703 105703.

[24]. Khan F, Khan A, Tuhin MO, Rabnawaz M, Li Z, Naveed M, A novel dual-layer approach towards omniphobic polyurethane coatings, RSC Adv9 (2019) 26703–26711, 10.1039/C9RA04923A.

[25]. Ghasemlou M, Daver F, Ivanova EP, Adhikari B, Bio-inspired sustainable and durable superhydrophobic materials: from nature to market, J. Mater. Chem. A7 (2019) 16643–16670, 10.1039/C9TA05185F.

[26]. Zhao X, Park DS, Choi J, Park S, Soper SA, Murphy MC, Robust, transparent, superhydrophobic coatings using novel hydrophobic/hydrophilic dual-sized silica particles, J. Colloid Interface Sci574 (2020), 10.1016/j.jcis.2020.04.065.

[27]. Wu M, Chen Y, Lin H, Zhao L, Shen L, Li R, Xu Y, Hong H, He Y, Membrane fouling caused by biological foams in a submerged membrane bioreactor: Mechanism insights, Water Res (2020), 10.1016/j.watres.2020.115932.

[28]. Sun T, Liu Y, Shen L, Xu Y, Li R, Huang L, Lin H, Magnetic field assisted arrangement of photocatalytic TiO2 particles on membrane surface to enhance membrane antifouling performance for water treatment, J. Colloid Interface Sci (2020), 10.1016/j.jcis.2020.03.008.

[29]. Liu Y, Shen L, Lin H, Yu W, Xu Y, Li R, Sun T, He Y, A novel strategy based on magnetic field assisted preparation of magnetic and photocatalytic membranes with improved performance, J. Memb. Sci (2020), 10.1016/j.memsci.2020.118378.

[30]. Blaga A, Use of plastics in solar energy applications, Sol. Energy21 (1978), 10.1016/0038-092X(78)90010-5.

[31]. Sollier E, Murray C, Maoddi P, Di Carlo D, Rapid prototyping polymers for microfluidic devices and high pressure injections, Lab Chip11 (2011), 10.1039/c1lc20514e.

[32]. Zhao X, Park D-S-W, Soper SA, Murphy MC, Microfluidic Gasketless Interconnects Sealed by Superhydrophobic Surfaces, J. Microelectromechanical Syst (2020) 1–6, 10.1109/JMEMS.2020.3000325.

[33]. Young III T, An essay on the cohesion of fluids, Philos. Trans. R. Soc. London95 (1805) 65–87, 10.1098/rstl.1805.0005.

[34]. Wang YX, Wu YP, Li WJ, Zhang LQ, Influence of filler type on wet skid resistance of SSBR/BR composites: Effects from roughness and micro-hardness of rubber surface, Appl. Surf. Sci257 (2011), 10.1016/j.apsusc.2010.08.129.

[35]. Jeong HE, Kwak MK, Park CI, Suh KY, Wettability of nanoengineered dual-roughness surfaces fabricated by UV-assisted capillary force lithography, J. Colloid Interface Sci339 (2009) 202–207, 10.1016/j.jcis.2009.07.020. [PubMed: 19656522]

[36]. Kwon Y, Patankar N, Choi J, Lee J, Design of surface hierarchy for extreme hydrophobicity, Langmuir25 (2009) 6129–6136, 10.1021/la803249t. [PubMed: 19466776]

[37]. Cortese B, D'Amone S, Manca M, Viola I, Cingolani R, Gigli G, Superhydrophobicity due to the hierarchical scale roughness of PDMS surfaces, Langmuir24 (2008) 2712–2718, 10.1021/la702764x. [PubMed: 18217778]

[38]. Sung YH, Kim YD, Choi HJ, Shin R, Kang S, Lee H, Fabrication of superhydrophobic surfaces with nano-in-micro structures using UV-nanoimprint lithography and thermal shrinkage films, Appl. Surf. Sci349 (2015) 169–173, 10.1016/j.apsusc.2015.04.141.

[39]. Wagterveld RM, Berendsen CWJ, Bouaidat S, Jonsmann J, Ultralow hysteresis superhydrophobic surfaces by excimer laser modification of SU-8, Langmuir22 (2006) 10904–10908, 10.1021/la0620298. [PubMed: 17154561]

[40]. Xu QF, Liu Y, Lin FJ, Mondal B, Lyons AM, Superhydrophobic TiO2-polymer nanocomposite surface with UV-induced reversible wettability and self-cleaning properties, ACS Appl. Mater. Interfaces5 (2013) 8915–8924, 10.1021/am401668y. [PubMed: 23889192]

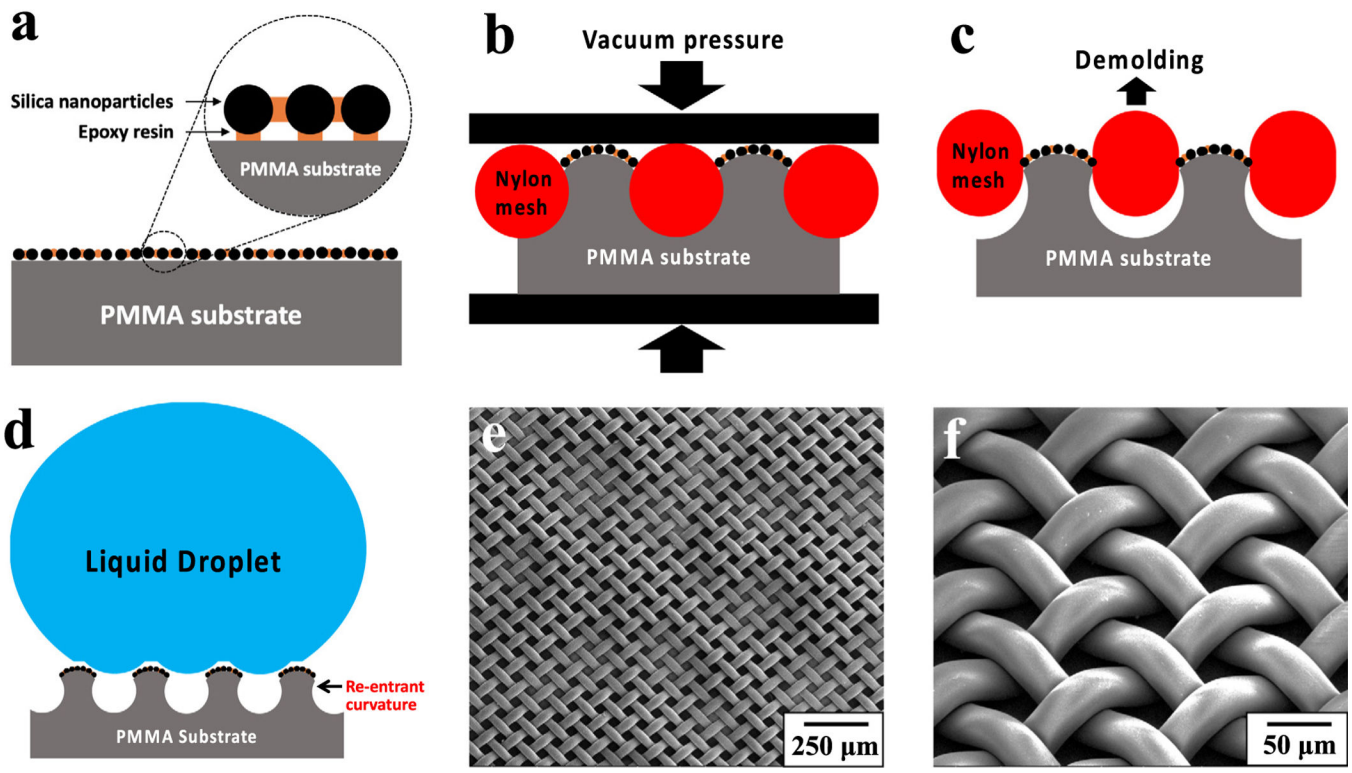

Fig. 1.

Schematics of (a) spin coating a mixture of silica nanoparticles and epoxy resin on PMMA substrate, (b) imprinting molding process using nylon-mesh as a template, (c) demolding of nylon-mesh template from PMMA substrate, (d) the obtained PMMA substrate exhibited re-entrant surface curvature with microscopic air trapped beneath a liquid droplet, and (e, f) SEM images of nylon-mesh template.

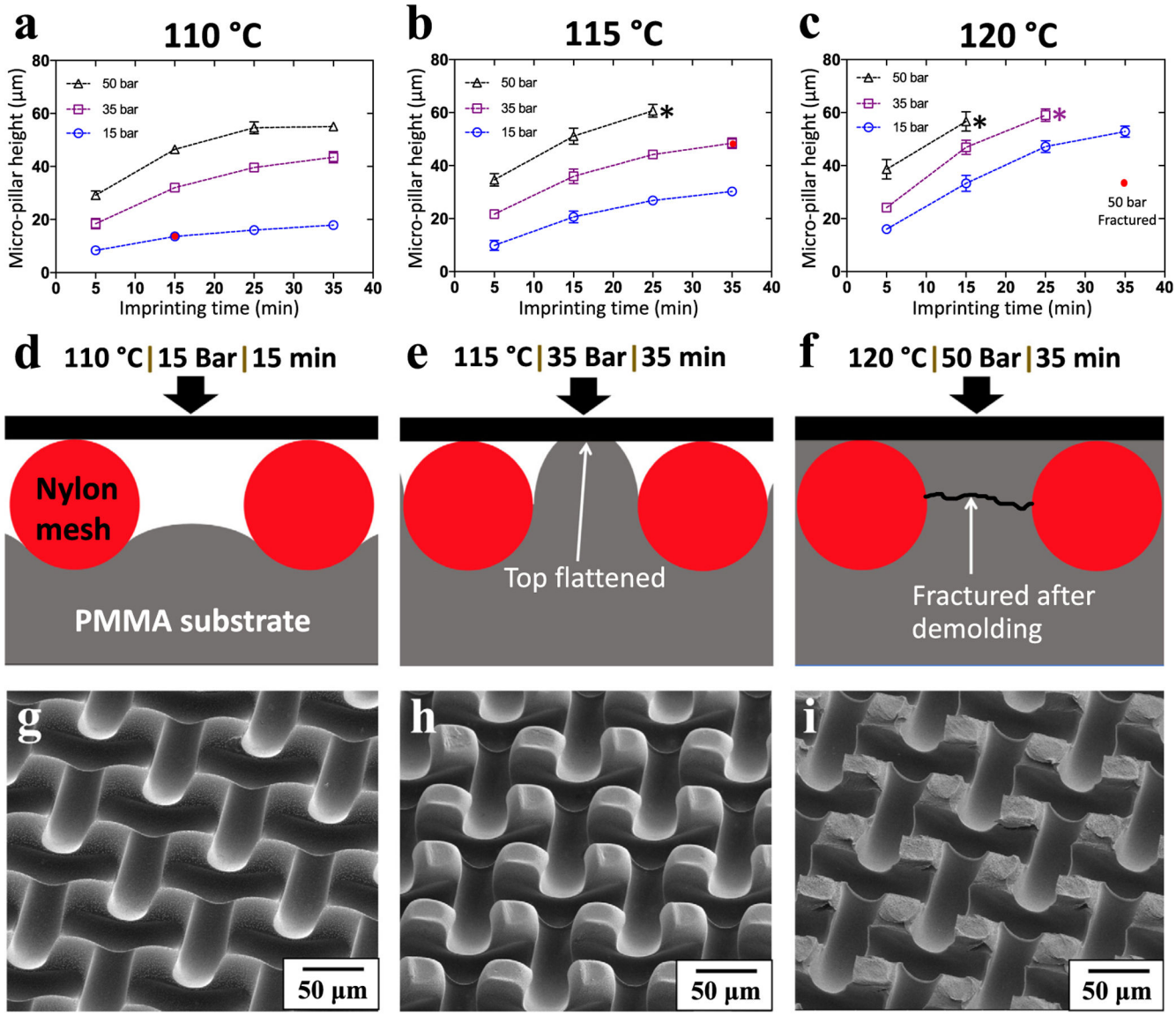

Fig. 2.

The micro-pillar height vs. imprinting time at (a) 110 °C, (b) 115 °C, and (c) 120 °C, respectively. The asterisks in (b, c) denote the maximum imprinting time without fracturing the micro-pillars during demolding. Schematics and SEM images showing the (d, g) incomplete molding, (e, h) flattening of the top micro-pillars, and (f, i) fracturing of micro-pillars during demolding, in which the imprinting parameters (time, pressure, and temperature) were highlighted as red dots in (a), (b), and (c), respectively.

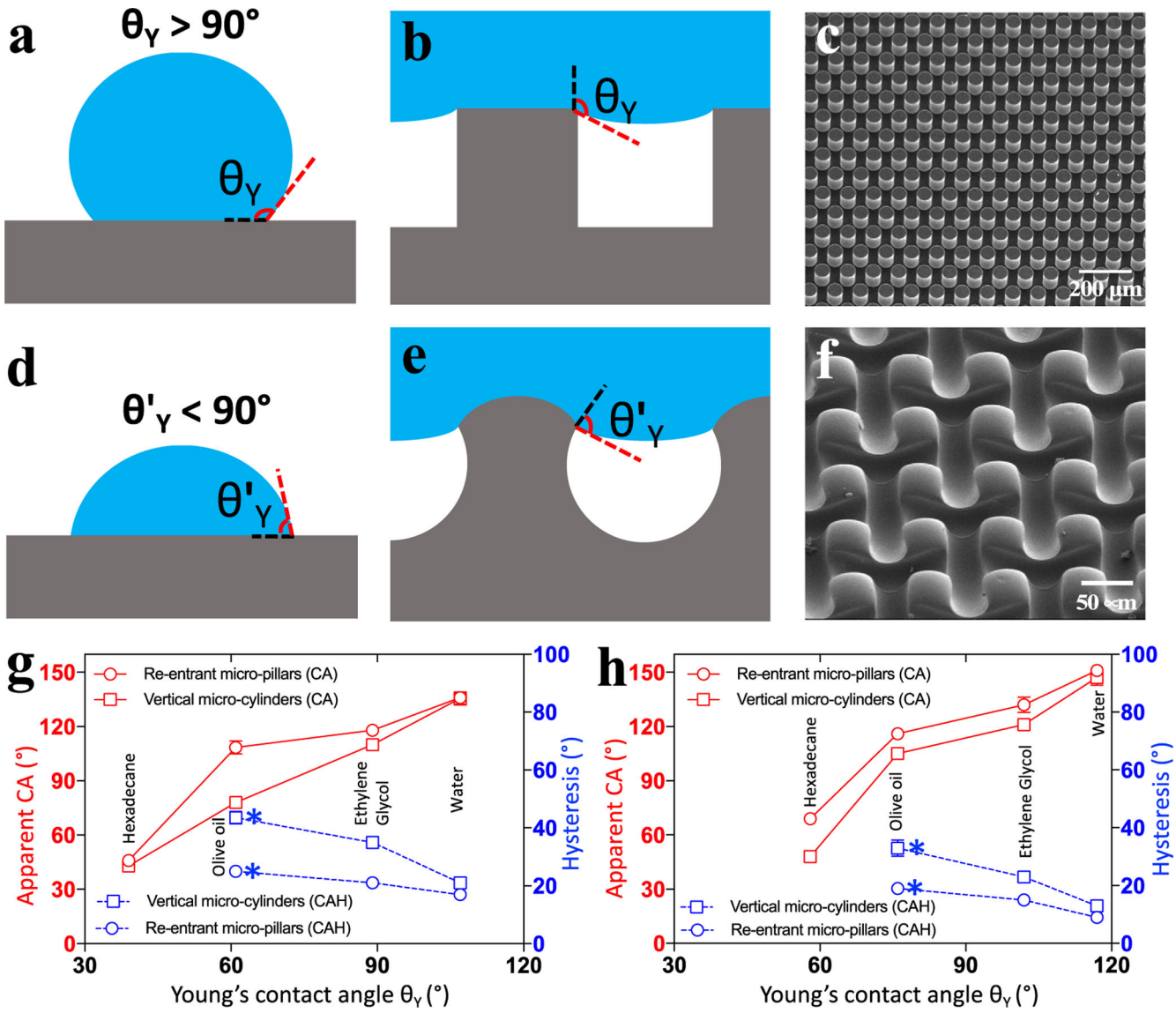

Fig. 3.

Schematics of (a, b) high and (d, e) low surface tension liquids on the flat and vertical micro-cylindered surfaces, respectively. SEM images of (c) micro-cylindered and (d) re-entrant surfaces. The measured apparent CA and hysteresis vs. young's contact angle of various liquids on the re-entrant micro-pillars, post-treated with (g) trichloro-octadecylsilane (OTS) and (h) perfluorodecyltrichlorosilane (FDTS). The asterisks in (g, h) denote the minimum Young's contact angle for a measurable hysteresis.

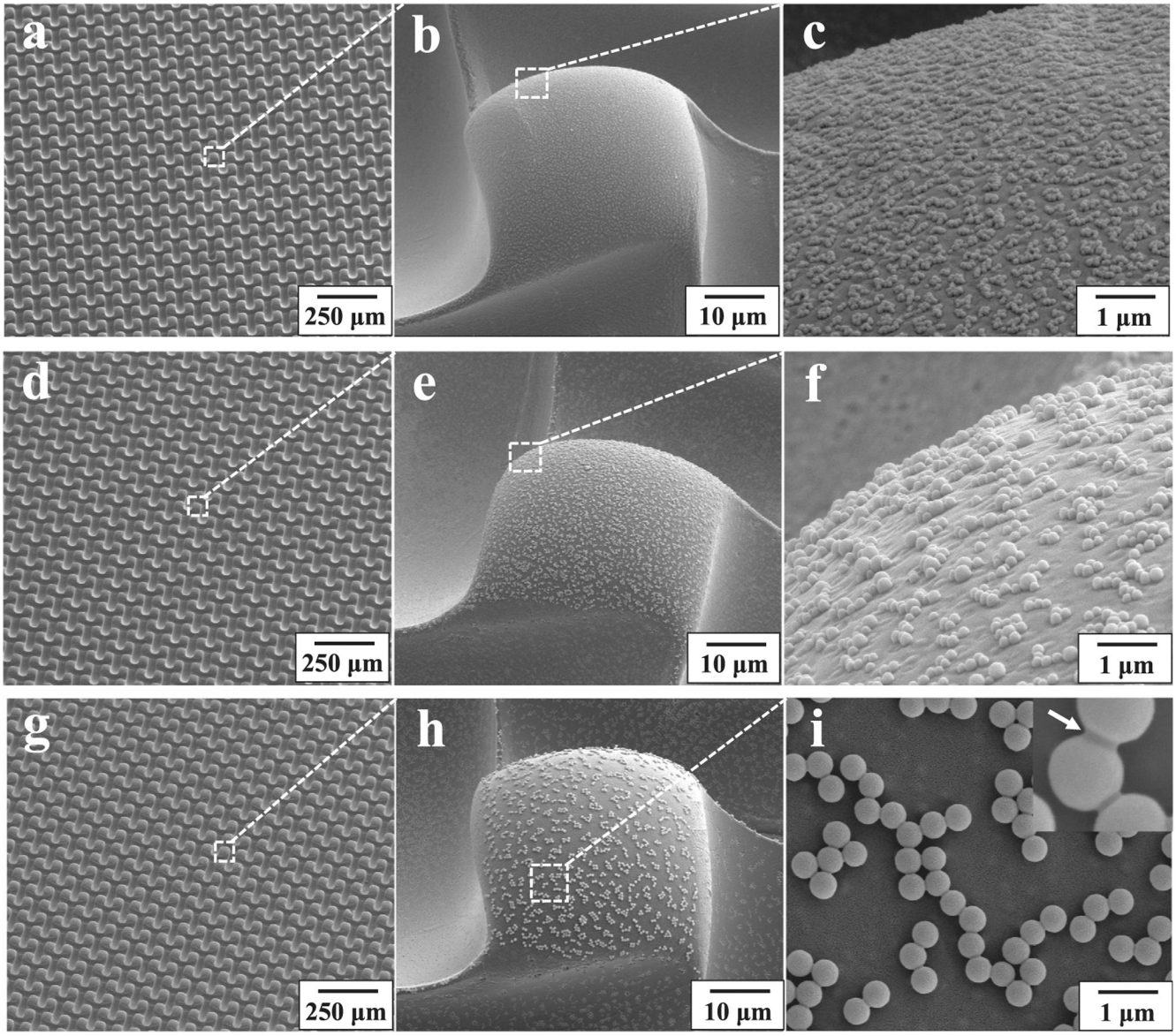

Fig. 4.

SEM images of 70 nm (a-c), 200 nm (d-f) and 400 nm (g-i) silica particles, along with epoxy resin binder, on nylon-mesh templated micropillar structures. Inset in (i) shows 400 nm silica particles connected with epoxy resin bridges.

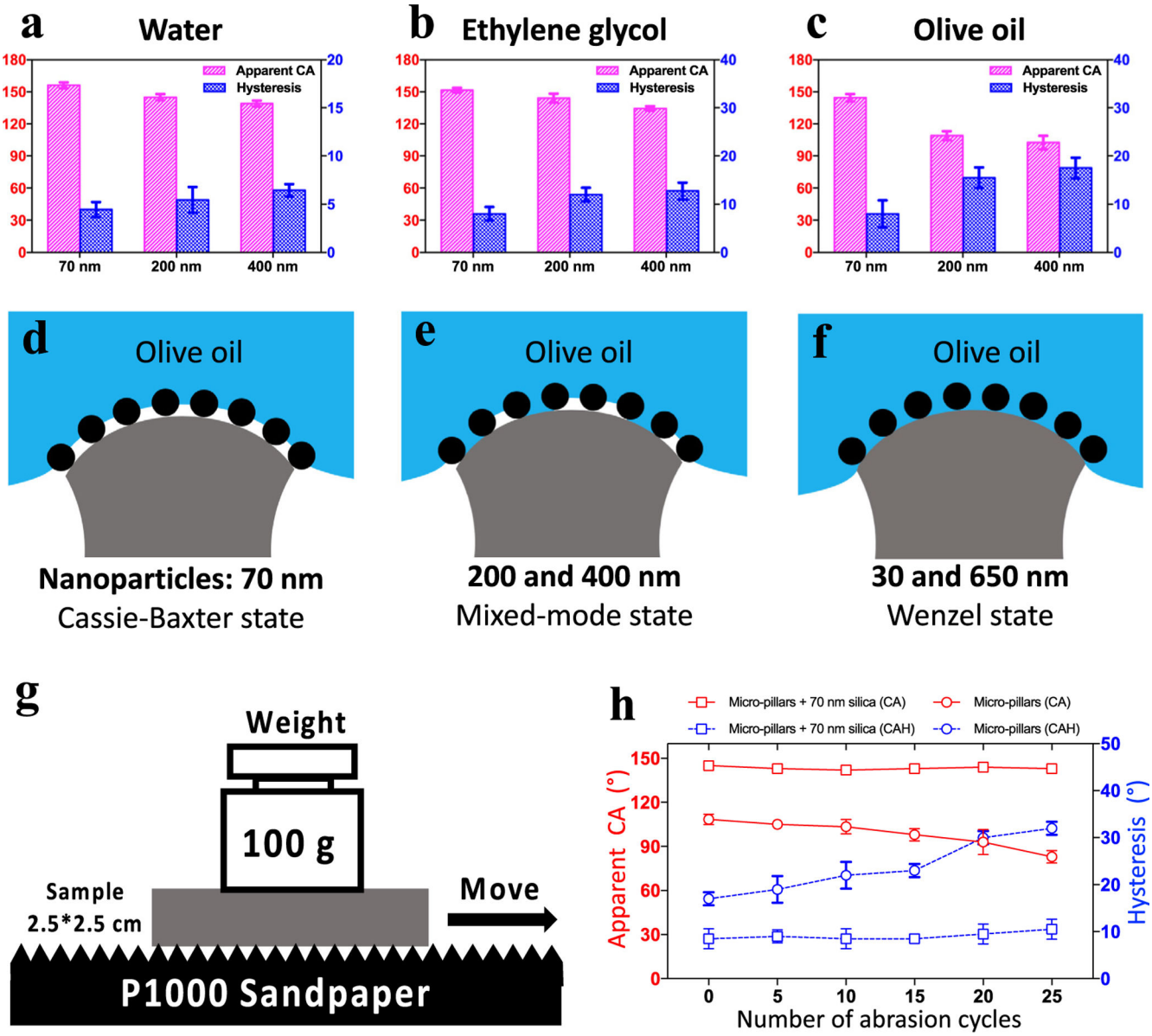

Fig. 5.

The measured apparent CA and hysteresis of (a) water, (b) ethylene glycol, and (c) olive oil on the obtained fluorine-free, trichloro-octadecylsilane (OTS) treated PMMA surfaces. The (d) Cassie-Baxter state (70 nm silica), (e) mixed-mode state (200 and 400 nm silica), and (f) Wenzel state (30 and 650 nm silica) of the nano-textured micro-pillar surfaces. (g) Schematic showing the P1000 sandpaper abrasion test on the omniphobic PMMA surfaces, and (h) the measured apparent CA and hysteresis of olive oil on bare and 70 nm silica coated re-entrant PMMA surfaces.